Data Repository Item

Methodological Details and Supplementary Data

Soreghan, Soreghan, Poulsen, Young, Eble, Sweet, & Davogustto

"Anomalous Cold in the Pangaean Tropics"

GPS Locations

For outcrop (1) and borehole (2) locations cited in the manuscript (Figure 1):

(1) 38°46.354 N, 108°53.024 W and 38°36.291 N, 108°53.061 W

(2) 38°46.052 N, 108°48.861 W

Gravity Analyses

The gravity survey used a LaCoste-Romberg Type D gravimeter. The station interval was 32 m (Figure DR1), and the station locations were determined by differential GPS measurements. Three gravity observations were averaged at each station, and a linear-drift correction applied. The reduced free-air gravity anomaly included a free-air correction, a latitude correction and a tidal correction as detailed below. The program GM-SYS was used in 2 ½ D gravity modeling mode and accounted for canyon topography over a 3 km cross-section centered on the Massey #1 well. The standard value for basement density, 2.67 gm/cc, was chosen, and an optimal density for the fill, 1.93 gm/cc, was determined by modeling. Velocities from a nearby shallow refraction/reflection seismic survey (see Fig. DR1 and Suarez, 2007) were consistent with the densities used in gravity modeling.

Drift Correction—For the linear drift correction, we established a base station, recorded readings here at the beginning and end of the survey and used the difference:

$$dc_s = \frac{g_{obsb2} - g_{obsb1}}{t_{b2} - t_{b1}}\left(t_s - t_{b1}\right)$$

Where dc_s is the drift correction for the station, tb1 and t_{b2} are the times at the start and the end of the survey in the base station, gobs are the null readings at the base and t_s is the time at the station.

Latitude Correction--The latitude correction is obtained by differentiating the international gravity formula with respect to latitude:

$$Lc = \left(1/R_e\right)\Delta g_t / \Delta\phi$$

$$Lc = 0.811\sin\left(2\phi\right)\Delta S \text{ mGal/ Km}$$

Where φ is the latitude, ΔS is the horizontal distance from the base station. The correction is always added to g as one moves toward the equator.

Free Air Correction—We accounted for elevational changes between stations by reducing all to a common datum. The Free air correction is then obtained by deriving the scalar equation of the gravity acceleration with respect the radial distance:

$$c_{fa} = 2g/R_e$$

$$c_{fa} = 0.3086h \text{ mGal/m}$$

The free air correction is added to or subtracted from the field reading depending on whether the station is above or below the datum, respectively.

Bouguer Correction--The Bouguer correction accounts for the mass between the datum surface and the stations and is given by:

$$c_b = 2\pi G\rho h$$

$$c_b = 0.04192\rho h \text{ mGal/m}$$

Terrain Correction--The terrain correction accounts for topographic undulations in regions surrounding each station. Using a detailed topographic map we divided the nearby region using concentric circles and radial lines to construct sectors whose areas increase with distance from the station; then the gravity effect of each sector is calculated from the formula:

$$T_g = G\rho\theta\left[(r_0 - r_i) + \left(r^2{}_i + \Delta z^2\right)^{/2} - \left(r^2{}_0 + \Delta z^2\right)^{/2}\right]$$

Figure DR1: Location map for gravity profiles in western Unaweep Canyon (see Figure 1 of manuscript for additional location information). Note that two profiles were conducted (A and B). Profile A is highlighted as these link to well results, but results for Profile B match those for Profile A in exhibiting a U-shaped basement as a best fit. Topographic bases are portions of the Fish Creek (Colorado) 7 ½ -minute quad (U.S. Geological Survey, 1972) and the Two V Basin (Colorado) 7 ½ -minute quad (U.S. Geological Survey, 1969).

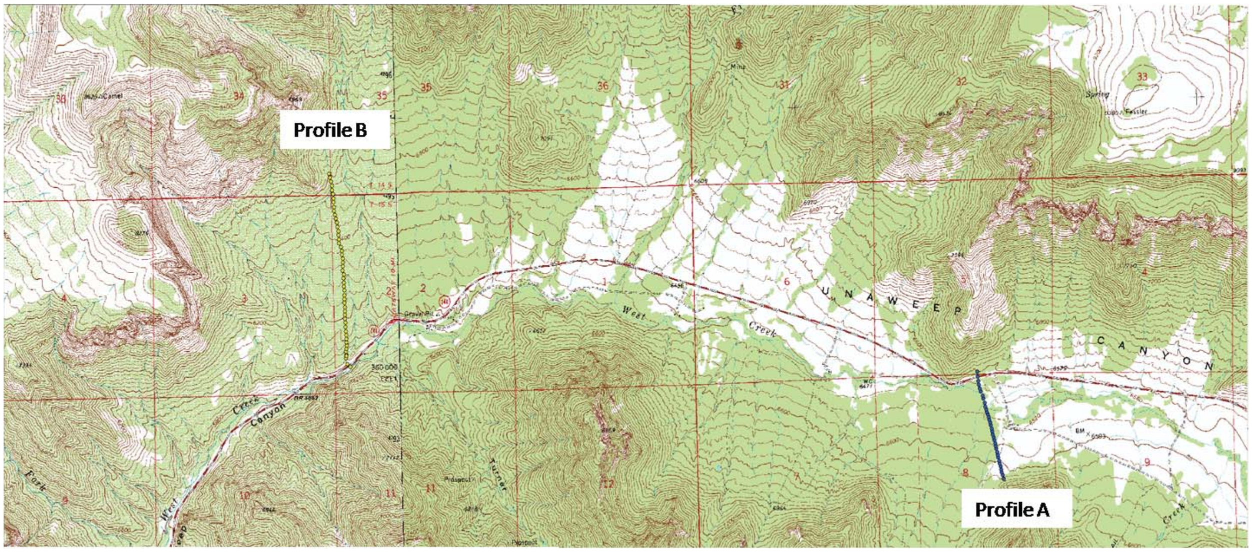
Profile B
Profile A
UNAWEEP
CANYON
West Creek

Table DR1: Gravity Data for Profile "A"

Station	Easting (m)	Northing (m)	Elevation (m)	Dial Reading	Time	Time (min)	Correction (mGal)	Corrected (mGal)	Dial Converted (mGal)	Latitude Correction (mGal)	Free Air Correction (mGal)
G-1	690061.112	4292614.622	2030.918	3041.810	10:32	19	-0.130	3192.402	3192.532	0.351856137	11.941776
G-2	690053.028	4292643.523	2019.809	3043.760	10:48	35	-0.239	3194.339	3194.578	0.328901348	8.520204
G-3	690047.101	4292667.731	2018.602	3044.095	10:53	40	-0.274	3194.656	3194.930	0.309674003	8.148448
G-4	690040.630	4292691.723	2016.958	3044.230	11:02	49	-0.335	3194.736	3195.072	0.290618216	7.642096
G-5	690034.056	4292715.562	2015.156	3044.225	11:11	58	-0.397	3194.670	3195.066	0.271683951	7.08708
G-6	690027.438	4292739.362	2013.360	3044.495	11:21	68	-0.465	3194.885	3195.350	0.252780662	6.533912
G-7	690021.413	4292763.248	2011.265	3045.000	11:32	79	-0.540	3195.339	3195.880	0.233809066	5.888652
G-8	690015.156	4292787.518	2009.622	3045.105	11:51	98	-0.670	3195.320	3195.990	0.214532477	5.382608
G-9	690008.681	4292811.416	2006.980	3045.615	11:58	105	-0.718	3195.807	3196.525	0.195551351	4.568872
G-10	690002.712	4292835.727	2005.172	3045.635	12:08	115	-0.787	3195.759	3196.546	0.176242196	4.012008
G-11	689996.286	4292859.870	2003.249	3046.250	12:41	148	-1.013	3196.179	3197.192	0.157066477	3.419724
G-12	689990.198	4292883.978	2001.301	3046.600	12:49	156	-1.067	3196.492	3197.559	0.137918557	2.81974
G-13	689984.158	4292908.115	2000.329	3046.895	12:53	160	-1.095	3196.774	3197.869	0.118747604	2.520364
G-14	689977.999	4292932.276	1998.783	3046.970	13:00	167	-1.142	3196.805	3197.947	0.099557588	2.044196
G-15	689971.562	4292956.492	1996.353	3047.400	13:13	180	-1.231	3197.167	3198.399	0.080323889	1.295756
G-16	689965.069	4292980.575	1996.185	3047.545	13:34	10	-0.061	3197.183	3198.551	0.061195825	1.244012
G-17	689958.779	4293004.385	1994.957	3047.825	13:42	18	-0.111	3197.427	3198.845	0.042284593	0.865788
G-18	689952.724	4293028.730	1993.617	3048.185	13:53	29	-0.178	3197.738	3199.223	0.022948434	0.453068
G-19 (Datum)	689945.288	4293057.623	1992.146	3048.550	13:59	35	-0.215	3198.084	3199.606	0	0
G-20	689940.432	4293076.980	1990.712	3048.800	14:09	45	-0.276	3198.285	3199.868	-0.015374411	-0.441672
G-21	689933.783	4293100.965	1989.632	3049.100	14:18	54	-0.332	3198.545	3200.183	-0.034424637	-0.774312
G-22	689927.121	4293124.627	1987.781	3049.550	14:28	64	-0.393	3198.955	3200.655	-0.053218319	-1.34442
G-23	689920.147	4293145.727	1987.147	3049.930	14:42	78	-0.479	3199.268	3201.054	-0.069977118	-1.539692
G-24	689910.033	4293165.737	1984.628	3050.660	14:49	85	-0.522	3199.991	3201.820	-0.085870177	-2.315544
G-25	689903.628	4293187.335	1983.640	3050.790	15:06	102	-0.627	3200.023	3201.957	-0.103024515	-2.619848
G-26	689897.469	4293209.921	1981.268	3051.455	15:18	114	-0.700	3200.648	3202.655	-0.120963578	-3.350424
G-27	689890.673	4293240.493	1979.285	3052.280	15:38	134	-0.823	3201.391	3203.520	-0.145245568	-3.961188
G-28	689880.096	4293277.366	1978.738	3052.525	15:48	144	-0.884	3201.586	3203.778	-0.174532164	-4.129664
G-29	689871.683	4293301.226	1978.188	3053.100	15:56	152	-0.934	3202.141	3204.381	-0.193483108	-4.299064
G-30	689857.189	4293333.885	1977.183	3053.360	16:06	162	-0.995	3202.352	3204.654	-0.21942271	-4.608604

Station	Easting (m)	Northing (m)	Elevation (m)	Dial Reading	Time	Time (min)	Correction (mGal)	Corrected (mGal)	Dial Converted (mGal)	Latitude Correction (mGal)	Free Air Correction (mGal)
G-31	689844.456	4293359.644	1978.640	3053.540	10:11	17	0.019	3203.555	3204.843	-0.239881947	-4.159848
G-32	689837.539	4293390.637	1981.016	3053.260	10:29	35	0.039	3203.281	3204.549	-0.264498318	-3.42804
G-33	689832.970	4293421.808	1987.364	3052.120	10:42	48	0.054	3202.099	3203.353	-0.289256067	-1.472856
G-34	689826.886	4293455.205	1996.005	3051.250	10:54	60	0.067	3201.200	3202.439	-0.31578183	1.188572
G-35	689823.110	4293495.814	2006.005	3049.745	11:06	72	0.080	3199.634	3200.860	-0.348035766	4.268572
Base	689932.727	4293104.603	1989.525	3050.255	10:13	0	0.000	3201.395	3201.395	-0.03731414	-0.807268
Base	689932.727	4293104.603	1989.525	3049.010	13:24	191	-1.307	3198.782	3200.088	-0.03731414	-0.807268
Base	689932.727	4293104.603	1989.525	3049.225	16:20	176	-1.081	3199.233	3200.314	-0.03731414	-0.807268
Base	689932.727	4293104.603	1989.525	3049.305	9:54	0	0.000	3200.398	3200.398	-0.03731414	-0.807268
Base	689932.727	4293104.603	1989.525	3049.405	11:28	94	0.105	3200.608	3200.503	-0.03731414	-0.807268

Palynology

Palynological results from outcrop and core samples are also reported in Soreghan et al. (2007). Figure DR2 illustrates representative Paleozoic palynomorphs recovered from the basal diamictite encountered in core from the Massey well (point 2 on Fig. 1). All samples were processed and analyzed by C.F. Eble at the Kentucky Geological Survey. Multiple sample splits were processed, each time using virgin sample containers, to exclude the possibility of contamination. The recovered palynomorph assemblage is indicative of Late Pennsylvanian-Early Permian age, and most probably Early Permian.

Figure DR2: Photomicrographs of palynomorphs: (A) Vesicaspora wilsonii (long axis 67 μm; (B) Florinites (long axis 45 μm); (C) Endosporites globiformis (long axis 90 μm); (D Thymospora thiessenii (long axis 23 μm); (E) Laevigatosporites minor (long axis 43 μm); (F) Lycospora granulata (long axis 39 μm).

Vesicaspora wilsonii

Florinites (degraded)

Endosporites globiformis

Thymospora thiessenii

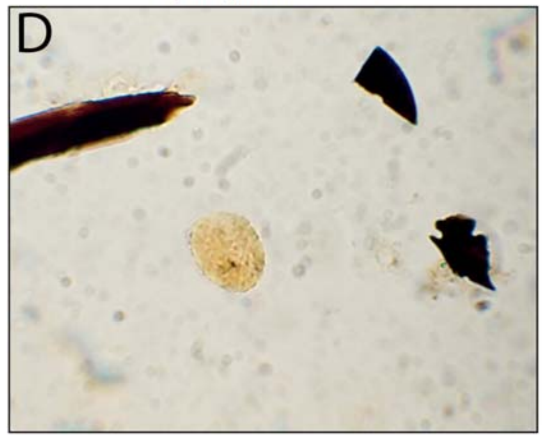

Laevigatosporites minor (degraded condition)

Lycospora granulata

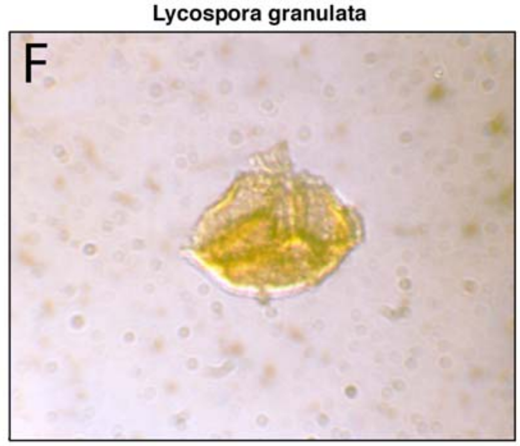

Scanning Electron Microscopy (SEM)

Four samples of poorly consolidated upper Paleozoic diamictite were processed to clean and isolate quartz for SEM analysis of surface textures. Two of the samples are from the diamictite exposed in western Unaweep Canyon (point 1 on Fig. 1), and two are from the diamictite recovered in the core (315.3 and 318.2 m depths) from the Massey well (point 2 on Fig. 1). Samples were disaggregated by immersion in a dilute dispersant of sodium carbonate and subsequently treated with the citrate-bicarbonate-diothionite (CBD) method to remove iron oxides (Mehra and Jackson, 1960; Janitzky, 1986). After sieving to isolate the coarse-grained (500-2000 μm) sand fraction, 16-22 quartz grains per sample were randomly selected and mounted for detailed examination on a scanning electron microscope (SEM, Zeiss DSM-960A). Microtextures were identified and logged following established standards and techniques (Mahaney, 2002). All features logged exhibit slight to moderate precipitation coatings, indicating their antiquity (Fig. 2F). Occurrence frequency of features is tabulated in Table DR2 (categories from Mahaney, 2002) where data from Mahaney and Kalm (2000) are also tabulated for comparison. Several authors have established that some microtextures uniquely identify specific transport processes (references below). For example, gouges, grooves and troughs reflect grain-to-grain contact under high-stress conditions, most characteristic of glacial till of varying geologic age (Mahaney et al., 1996; Mahaney and Kalm, 2000; Mahaney, 2002; Van Hoesen et al., 2004). In contrast, v-shaped cracks, edge rounding and breakage blocks reflect fracturing formed by percussion (i.e., saltation) dominant in fluvial systems (Mahaney and Kalm, 2000). Finally, polygenetic textures are those produced under a variety of conditions, such as conchoidal fractures that could reflect either grain crushing in a glacial environment or grain fracturing in a fluvial environment (Mahaney, 2002). Hence, the textural classification into 'high-stress,' 'percussion,' and 'polygenetic' categories enables a graphical simplification of textures meant to highlight processes most indicative of glacial versus fluvial environments.

Table DR2: Tabulation of SEM microtextures on sand-sized quartz

	Grains examined (N)	fracture faces	subparallel linear fractures	conchoidal fractures	sharp angular features	arc shaped steps	linear steps	abrasion features	crescentic gouges	straight grooves	curved grooves	deep troughs	mechanically-upturned plates	v-shaped percusssion scars	edge rounding	breakage blocks	dissolution etching	weathered surfaces	low relief	medium relief	high relief
Unaweep diamictite																					
CUTS I-8	20	75	90	95	65	25	25	15	5	30	0	15	30	0	0	35	15	0	25	65	10
CUT B1	16	50	63	69	13	56	44	13	6	0	6	31	31	0	25	38	31	0	38	56	6
Unaweep 1044	20	45	80	85	45	55	20	55	25	35	5	25	50	0	0	25	80	0	20	55	25
Unaweep 1034.5	22	32	77	64	45	64	50	68	27	27	23	41	41	27	5	45	59	0	14	45	45
Devonian Fluvial(1)	N/A	3	8	6	0	0	0	52	0	0		0	0	60	63	N/A	44	40	58	38	8
Pleistocene Till(1)	N/A	2	47	52	47	3	15	47	0	14	11	21	18	20	18	N/A	19	2	7	21	57

Numeric data represents the presence of microtextures on grains, given in percentage. Orange columns are polygenetic textures, Blue columns are high-stress features, and Yellow columns are percussion textures.

(1) Data is from Mahaney and Kalm (2000)

Compilation of Gravel-Bed River (GBR) Gradients

Data compilations on GBRs from various regions show maximum slopes of 0.006 (range 0.0005-0.006, average=0.003, n=16) (Blair and McPherson, 1994) to .019 (range 0.0001-0.0190; average=0.0062, n=37) (Church and Rood, 1983). Reported slopes for various reaches of nonbraided GBRs in the modern Rocky Mountains range between 0.00088-0.026 (average=0.0084, n=24), with only two measurements exceeding 0.02 (Andrews, 1984). If the proximal Cutler Formation represents a proglacial system, as proposed by Soreghan et al. (2005), the slopes remain similar. Today, proglacial systems that reach to sea level exist only in mid- to high-latitude regions; these systems can be very steep (.02-.07) within a few km of the ice margin, but follow highly concave profiles such that typical distal gradients are in the 10^{-3} to 10^{-4} range, with average gradients <0.01 over the entire glacial-terminus to coastal-plain distance (Fahnestock, 1963; Boothroyd and Ashley, 1975). As reconstructed from DEM data, for example, the average gradient on the mid-latitude Nisqually River (Washington) from its inception at Nisqually Glacier to its coastal terminus 140 km distant is 0.0089. Figure DR3 shows the paleogeographic reconstructions for the Cutler system.

Figure DR3: Paleogeography of Uncompahgre-Paradox region during Cutler-Unaweep time, with distribution of lowstand (glacial) depositional systems and location of highstand (interglacial) shoreline positions (green dashed line; Condon, 1997). Multiple marine limestones within the lower Cutler Formation as represented from outcrop and well data (Condon, 1997) were used to constrain the maximal highstand position. A-A′ shows reconstructions of elevations at the ice terminus using a range of *average* depositional gradients (see text). Glacioeustatic amplitude shown at A is 100 m (Soreghan and Giles, 1999).

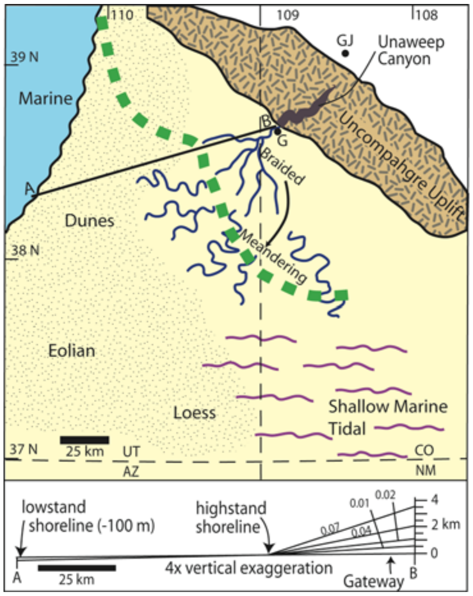

Loess Geochemistry

Pedogenically modified loessites are those displaying pedogenic features (e.g. ped structure, melanization, root traces, etc) such as outlined in Kessler et al. (1999), Soreghan et al., (2002) and Tramp et al. (2004). Samples coded as loessite are from the middle portions of loessite units and those coded as 'weathered loessite' occur immediately adjacent (within 20 cm) of a paleosol. The good correlation (r^2=0.74) of TiO_2 and Al_2O_3 within the paleosols and weathered loessite (Fig. 3B) indicates that these immobile elements become concentrated as weathering proceeds (Nesbitt and Young, 1998). However, the lack of such a correlation within the loessite indicates that the variability is created by source rock variation in TiO_2 and Al_2O_3. Note that the variation in Al_2O_3in loessite is much smaller compared to paleosols. Given the well-sorted nature of the loessite on average, the variability in $TiO_2$is less than that exhibited in glacial diamictite (Nesbitt and Young, 1998), but the trend is identical nonetheless.

Table DR 3: Geochemistry of Upper Paleozoic Loessites and Paleosols (in wt%)

Sample ID	Lithology[1]	Location[2]	SiO2	TiO2	Al2O3	Fe2O3	MgO	CaO	Na2O	K2O	P2O5	LOI
P bd-1	L	BD	83.24	0.55	7.34	1.53	0.33	0.1	1.72	2.69	0.02	1.15
P107.5	L	BD	83.7	0.56	6.43	1.54	0.27	0.01	1.65	2.53	0.06	3.51
P108.0	L	BD	82.6	0.54	6.87	0.41	0.27	0.66	1.61	2.73	0.05	1.24
P56.75	L	BD	83.79	0.54	7.4	1.58	0.3	0.13	1.3	3.05	0.02	0.88
P64.4	L	BD	88.01	0.4	6.13	0.87	0.18	0.12	1.33	2.42	0.01	0.62
LRR 011.0	L	CO	84.58	0.38	6.81	1.41	0.32	0.07	1.55	2.35	0.04	0.92
LRR 011.3	L	CO	84.68	0.45	6.66	1.47	0.31	0.07	1.55	2.27	0.04	0.96
LR20.5	L	CO	84.5	0.41	5.81	1.25	0.21	0.005	1.57	1.93	0.04	2.79
LR20.7	L	CO	82	0.53	6.86	1.63	0.33	0.1	1.7	2.28	0.005	2.32
LRR 26.8	L	CO	84.65	0.35	6.62	1.49	0.28	0.11	1.79	2.24	0.01	1.43
RR 013.2	L	CO	85.43	0.35	6.17	1.23	0.27	0.04	1.31	2.19	0.04	1.09
RR 031.2	L	CO	86.31	0.39	5.82	1.13	0.23	0.03	1.27	2.11	0.04	0.92
RR 041.3	L	CO	85.5	0.39	6.02	1.25	0.39	0.05	0.87	2.24	0.04	1.78
RR 065.65	L	CO	85.86	0.32	5.97	1.15	0.32	0.06	1.25	2.3	0.04	0.97
RR 129.5	L	CO	84.05	0.36	6.99	1.42	0.27	0.06	1.64	2.61	0.04	0.78
RR 153.9	L	CO	87.48	0.22	5.36	0.87	0.18	0.07	1.27	1.99	0.04	0.88
RR 179.1	L	CO	86.47	0.35	6.18	1.02	0.29	0.04	1.09	2.37	0.04	1.07
RR 198.8	L	CO	86.65	0.43	6.18	1.35	0.25	0.06	1.29	2.12	0.04	0.93
URR 011.6	L	CO	83.32	0.43	6.86	1.59	0.37	0.06	1.36	2.56	0.04	1.58
URR 023.0	L	CO	81.05	0.61	8.27	2.02	0.45	0.06	1.66	2.88	0.04	1.24
URR32	L	CO	86.64	0.5	5.93	1.26	0.28	0.08	0.98	2.26	0.005	1.07
URR33.5	L	CO	85.53	0.42	6.5	1.22	0.25	0.07	1.1	2.53	0.005	0.84
URR 034.5	L	CO	85.7	0.35	6.17	1.15	0.27	0.04	1.18	2.36	0.04	1.19
URR48.2	L	CO	84.17	0.45	7.49	1.72	0.52	0.09	1.16	3.1	0.005	1.14
URR 052.1	L	CO	82.97	0.51	6.97	1.7	0.52	0.11	1.35	2.69	0.04	1.77
M 1.6	L	CO	85.75	0.39	6.06	1.31	0.3	0.06	1.36	2.48	0.01	0.86
M1.6	L	CO	84.5	0.41	6.28	1.4	0.3	0.78	1.22	1.86	0.01	1.12
UM2.1	L	CO	87.01	0.32	5.8	1	0.14	0.05	1.19	2.17	0.005	0.62
M2.5	L	CO	84.3	0.39	6.36	1.43	0.31	0.1	1.46	2.54	0.005	2.69
URR 076.7	L	CO	83	0.48	7.3	1.66	0.34	0.05	1.46	2.66	0.04	1.16
URR 096.7	L	CO	83.86	0.53	7.04	1.58	0.32	0.04	1.49	2.54	0.04	1.06
URR 146.8	L	CO	85.5	0.24	6.63	1.09	0.29	0.04	1.45	2.6	0.04	0.75
URR 205.2	L	CO	86.53	0.36	6.16	1.24	0.21	0.04	1.62	2.1	0.04	0.53
URR 225.8	L	CO	85.28	0.5	6.44	1.43	0.23	0.04	1.83	1.9	0.04	0.67
URR 330	L	CO	86.26	0.34	5.86	1.12	0.28	0.05	1.08	1.96	0.04	1.32
URR360.2	L	CO	83.14	0.59	7.54	1.71	0.37	0.12	1.92	1.95	0.005	0.92
URR369	L	CO	82.63	0.62	8.03	1.9	0.41	0.1	1.91	2.09	0.005	1.04
P70.95	L	BD	86.42	0.62	6.5	1.2	0.29	0.13	1.27	2.32	0.01	0.86
P97.6	L	BD	84.05	0.45	7.47	1.71	0.53	0.09	1.14	3.06	0.005	0.95
P79.55	L(L)	BD	81.84	0.7	8.92	1.75	0.35	0.27	1.79	3.83	0.02	0.51
LR20.3	L(L)	CO	84.7	0.28	5.22	1.08	0.21	0.65	1.3	1.66	0.12	3.16
P54.0	L(L)	BD	81.5	0.75	7.95	1.92	0.42	0.17	1.43	3.02	0.02	1.19
URR 169.7	L(L)	CO	86.05	0.41	5.9	1.25	0.22	0.06	1.4	2.29	0.04	0.58
URR 183.4	L(L)	CO	85.61	0.37	6.14	1.37	0.33	0.05	1.34	2.38	0.04	0.75
URR347.7	L(L)	CO	90.25	0.23	4.56	0.73	0.15	0.05	0.9	1.68	0.005	0.66
URR357.5	L(L)	CO	80.43	0.71	8.81	2.42	0.55	0.11	1.78	2.58	0.02	1.65
URR364	L(L)	CO	83.62	0.6	7.29	1.77	0.36	0.07	1.65	2.23	0.005	0.96
UR 364	L(L)	CO	83.98	0.6	6.95	1.78	0.35	0.06	1.87	2.1	0.02	1.28
P19.35	P	BD	73.21	0.87	11.72	3.44	1.03	0.14	1.37	4.28	0.02	2.48
M3.3	P	CO	82.5	0.45	7.18	1.55	0.35	0.03	1.5	2.78	0.02	2.14
UR363.4	P	CO	80.8	0.62	8.01	1.95	0.39	0.28	2	2.4	0.01	2.1
UR363.8	P	CO	75.8	0.79	10.3	3.26	1	0.25	1.76	3.68	0.05	3.57
P107.8	P(W)	BD	77.6	0.71	9.28	2.99	0.79	0.8	1.42	3.41	0.04	3.57
P107.8	P(W)	BD	77.6	0.71	9.28	2.99	0.79	0.8	1.42	3.41	0.04	3.57
P41.25	P(W)	BD	76.12	0.83	11.11	3.25	0.91	0.17	1.34	3.23	0.03	2.44
P52.1	P(W)	BD	81.93	0.7	8.16	1.99	0.45	0.11	1.39	2.85	0.02	0.9
LR20.9	P(W)	CO	82.1	0.51	7.15	1.75	0.38	0.005	1.76	2.31	0.02	2.61
LRR30.25	P(W)	CO	80.52	0.38	8.48	2.05	1.36	0.26	0.9	3.5	0.08	2.23
LRR31.3	P(W)	CO	88.3	0.32	5.75	1.05	0.18	0.08	1.31	1.98	-0.01	0.91
LRR32.1	P(W)	CO	80.75	0.49	8.99	2.11	0.64	0.22	1.38	2.86	0.01	1.58
RR 106.7	P(W)	CO	86.41	0.29	6.33	1.27	0.26	0.06	1.57	2.25	0.04	0.83
M2.9	P(W)	CO	80.1	0.5	8.71	2.18	0.91	0.35	1.29	3.62	0.02	2.38
URR351.6	P(W)	CO	79.21	0.65	8.97	2.55	0.78	0.14	1.25	3.36	0.02	2.28

Note: (1) LIthology: L=Loessite; L(L)=Sample immediately above paleosol; P=Paleosol; and P(W)=Weakly Pedogenic.
(2) Locality represents sample site: BD=Bravo Dome region, NM (see Kessler et al., 2001 for stratigraphic details) and CO= near Basalt, CO (see Tramp, et al., 2004 for stratigraphic details). Data summarized from Soreghan and Soreghan, 2007.

Climate Modelling

Late Paleozoic experiments were completed using GENESIS AGCM version 2.3 coupled to a 3-D dynamic ice-sheet model. GENESIS consists of an AGCM coupled to multi-layer models of vegetation, soil or land ice, and snow, with spectral resolution of T31 (~3.75°) and 18 vertical layers (Thompson and Pollard, 1997). GENESIS is asynchronously coupled to a 3-D thermo-mechanical ice-sheet model (DeConto and Pollard, 2003) that is based on the vertically integrated continuity equation for ice mass. The ice geometry is determined by the surface mass balance, basal melting, and ice flow. Sea-surface temperatures and sea ice are computed using a 50-m slab ocean with diffusive heat. A series of Late Paleozoic experiments were completed with a range of atmospheric CO_2 and orbital settings (Horton et al., 2007). Here we report on a simulation that produces the maximum continental ice extent. The simulation uses a palaeogeography and palaeotopography from the Paleogeographic Atlas Project's reconstruction for the Sakmarian (see http://pgap.uchicago.edu), atmospheric CO_2 level of 140 ppmv, pre-industrial levels of CH_4 and N_2O, a 3% reduction in solar luminosity, and orbital settings that minimize Southern Hemisphere summer insolation (obliquity = 22°, eccentricity = 0.06, precession = 270°). Montañez et al. (2007) report atmospheric pCO_2 as low as 280 ppmv in the Late Paleozoic. We have used a value that represents one-half of this concentration, and is similar to Last Glacial Maximum values, in order to maximize glaciation. Specifying higher levels of atmospheric pCO_2 raise the minimum elevation that will sustain glaciation. In western equatorial Pangaea, palaeotopography is 500-1500 m owing to the Central Pangaean Mountains.

References

Andrews, E.D., 1984, Bed-material entrainment and hydraulic geometry of gravel-bed rivers in Colorado: Geological Society of America Bulletin, v. 95, p. 371-378.

Blair, T.C., and McPherson, J.G., 1994, Alluvial fans and their natural distinction from rivers based on morphology, hydraulic processes, sedimentary processes, and facies assemblages: Journal of Sedimentary Research, v. A64, p. 450-489.

Boothroyd, J.C., and Ashley, G.M., 1975, Processes, bar morphology, and sedimentary structures on braided outwash fans, northeastern Gulf of Alaska, in Jopling A.V. and McDonald, B.C., eds., Glaciofluvial and Glaciolacustrine Sedimentation: SEPM Special Publication no. 23, p. 193-222.

Church, M., and Rood, K., 1983, "Catalogue of Alluvial River Channel Regime Data" (Univ. British Columbia, Department of Geography, Vancouver).

Condon, S.M., 1997, Geology of the Pennsylvanian and Permian Cutler Group and Permian Kaibab Limestone in the Paradox Basin, Southeastern Utah and Southwestern Colorado U. S. Geological Survey Bulletin 2000-P, 46 p.

DeConto, R., and Pollard, D., 2003, A coupled climate-ice sheet modelling approach to the Early Cenozoic history of the Antarctic ice sheet Palaeogeography, Palaeoclimatology, Palaeoecology, v. 198, p. 39-52.

Fahnestock, R.K., 1963, Morphology and hydrology of a glacial stream, White River, Mount Rainier, Washington: U.S. Geological Survey Professional Paper 422-A, 70 p.

Horton, D.E., Poulsen, C.J., and Pollard, D., 2007, Orbital and CO2 forcing of late Paleozoic continental ice sheets, Geophysical Research Letters, v. 34, L19708, doi:10.1029/2007GL03188.

Janitzky, P., 1986, Laboratory methods: Citrate-bicarbonate-dithionite (CBD) extractable iron and aluminium, in M.J. Singer & P. Janitzky, eds., Field and Laboratory Procedures used in a Soil Chronosequence Study. U.S. Geological Survey Bulletin, B 1648, p. 38-41.

Mahaney, W.C., 2000 Atlas of Sand Grain Surface Textures and Applications: Oxford University Press, Oxford, U.K.

Mahaney, W.C., and Kalm, V., 2000, Comparative scanning electron microscopy study of oriented till blocks, glacial grains and Devonian sands in Estonia and Latvia: Boreas, v. 29, p. 35-51.

Mehra, O.P. & Jackson, M.L. Iron oxides removal from soils and clays. Dithionite-citrate systems buffered with sodium bicarbonate, in Swineford, A., Ed., Proceedings 7th National Conference on Clays and Clay Minerals, Pergamon Press, Washington, DC, p. 317-327.

Montañez, I.P., Tabor, N.J., Niemeier, D., DiMichele, W.A., Frank, T.D., Fielding, C.R., Isbell, J.L., BIrgenheier, L.P., and Rygel, M.C., 2007, CO_2-forced climate and vegetation instability during late Paleozoic deglaciation: Science, v. 315, p. 87-91, doi: 10.1126/science.1134207.

Soreghan, G.S., and Giles, K.A., 1999, Amplitudes of Late Pennsylvanian glacioeustasy: Geology, v. 27, p. 255-258.

Soreghan, G.S., Soreghan, M.J., Eble, C.F., Sweet, D., Davogustto, O., Young, R.A., and Elmore, R.D., 2005, Late Paleozoic deglaciation in western equatorial Pangaea: Eos Transactions, American Geophysical Union, v. 86 (52), Fall Meeting Supplement, Abstract T11D-0406.

Soreghan, G.S., Sweet, D.E., Marra, K.R., Eble, C.F., Soreghan, M.J., Elmore, R.D., Kaplan, S.A., and Blum, M.D., 2007, An exhumed Late Paleozoic canyon in the Rocky Mountains: Journal of Geology, v. 115, p. 473-481.

Suarez-Rojas, Y., 2007, Acquisition, Processing and Modeling of Shallow Seismic Refraction and Reflection Profiles: Unaweep Canyon, Colorado: M.S. Thesis, University of Oklahoma, Norman, Oklahoma, 135 p.

Thompson, S., and Pollard, D., 1997, Greenland and Antarctic mass balances for present and doubled atmospheric CO2 from GENESIS version-2 global climate model Journal of Climate, v. 10, p. 871-900.

Van Hoesen, J.G., and Orndorff, R.L., 2004, A comparative SEM study on the micromorphology of glacial and nonglacial clasts with varying age and lithology: Canadian Journal of Earth Sciences, v. 41, p. 1123-1139.